Journal of
Ceramic Science
and Technology

J. Ceram. Sci. Technol., **09** [2] 183-192 (2018)
DOI: 10.4416/JCST2017-00097
available online at: http://www.ceramic-science.com

Three-Dimensional Network ZnO/$BaFe_{12}O_{19}$ Composite Thick Films and their Microwave Absorption Properties

Y. Lin, J. Dong, Y. Liu, N. Han, L. Wang, H. Yang*, J. Wang

School of Materials Science and Engineering, Shaanxi
University of Science and Technology, Xi'an, 710021, China

received December 12, 2017; received in revised form February 2, 2018; accepted March 4, 2018

Abstract

ZnO/$BaFe_{12}O_{19}$ composite thick films with four different ZnO/$BaFe_{12}O_{19}$ mass fractions were synthesized with the tape-casting method in the presence of plate-like $BaFe_{12}O_{19}$ grains and sphere-like ZnO grains. Their phase composition, morphology and magnetic properties were analyzed by means of XRD, SEM and VSM, respectively. The microwave absorption properties were also investigated in the frequency range of 2 – 18 GHz, and the results show that the ZnO/$BaFe_{12}O_{19}$ composite thick films have multiple microwave attenuation peaks and their microwave absorption properties can be easily tuned by varying the mass ratio of $BaFe_{12}O_{19}$/ZnO. When the mass ratio of $BaFe_{12}O_{19}$ to ZnO is 15:85, the composite thick film exhibits a minimum RL of -48.6 dB at 17.2 GHz with a thickness of 4.5 mm. The electromagnetic performance of the ZnO/$BaFe_{12}O_{19}$ composite thick films could be attributed to the effective complementarities between the dielectric loss and the magnetic loss.

Keywords: Tape casting, impedance matching, microwave absorption

I. Introduction

Microwave-absorbing materials have attracted growing attention because of their important applications in protecting the environment from the radiation of telecommunication equipment, and in some specific aircraft, communication devices, etc. [1–6]. ZnO is considered to be a promising microwave-absorbing material in civilian and military applications because of its light weight, low cost, simple synthesis, and strong absorption ability [7–11]. However, pure dielectric materials with high dielectric constants are harmful for impedance matching, which leads to strong reflection and weak absorption. Therefore, researchers are urged to find new types of electromagnetic-absorbing materials to deal with electromagnetic radiation.

The introduction of magnetic materials to form ZnO-based composites is a good solution to make up for the deficiency of ZnO. Recently, an increasing number of reports have focused on synthesizing ZnO-based composites because of their unique properties with possible technological applications in the microwave absorption field [12, 13]; these include, for example, $SrFe_{12}O_{19}$/ZnO [14], ZnO/$CoFe_2O_4$ [15] and $ZnAl_2O_4$/ZnO [16]. To the best of our knowledge, there are few reports on combining ZnO and $BaFe_{12}O_{19}$ to form composites. M-type Ba-hexaferrite ($BaFe_{12}O_{19}$) is a promising microwave-absorbing material owing to its axis-anisotropy behavior and magnetization value at the microwave frequencies [17–19]. Furthermore, its magnetic and dielectric properties could be modulated to satisfy different applications.

So far, various methods have been reported for synthesizing ZnO-based composites, such as the *in-situ* hydrolysis method [14], sol-gel process [15, 16] and hydrothermal method [20]. However, the above methods have many disadvantages such as expensive instruments, harsh reaction conditions, toxic reagents and long reaction time. Therefore, it is necessary to explore a simple, fast and low-cost method for the synthesis of ZnO-based composites. The tape-casting method has been demonstrated to be one of the more simple and feasible methods [14–16, 20]. The tape-casting method can also be easily adapted to prepare multi-layer composites. In this paper, ZnO/$BaFe_{12}O_{19}$ composite thick films with different mass ratios of $BaFe_{12}O_{19}$ were prepared with the tape-casting method [21–24]. The phase composition, morphology and microwave absorption properties of ZnO/$BaFe_{12}O_{19}$ composite thick films were also investigated in detail.

II. Experimental

(1) Materials

Barium carbonate ($BaCO_3$), iron sesquioxide (Fe_2O_3), sodium chloride (NaCl), barium chloride dihydrate ($BaCl_2{\cdot}2H_2O$), zinc nitrate hexahydrate ($Zn(NO_3)_2{\cdot}6H_2O$) and sodium carbonate ($NaCO_3$), glycerol trioleate, polyvinyl butyral (PVB), dibutyl phthalate and anhydrous ethanol were purchased from Sinopharm Chemical Reagent Co., Ltd. All the chemical reagents used in this study were of analytical pure grade and used without further purification.

(2) Synthesis of ZnO/$BaFe_{12}O_{19}$ composite thick films

The plate-like $BaFe_{12}O_{19}$ powders were synthesized with a two-step molten salt method (MSM). Firstly, Ba-

* Corresponding author: yanghaibo@sust.edu.cn

CO_3 and Fe_2O_3 were mixed according to the stoichiometric ratio of $BaFe_{12}O_{19}$. The mixed powders were calcined at 1000 °C for 2 h together with NaCl at the weight ratio of 1:2. The molten salt was washed with hot deionized water. Secondly, to coarsen the plate-like $BaFe_{12}O_{19}$ powders obtained from the MSM, the obtained powders were mixed with $BaCl_2{\cdot}2H_2O$ and Fe_2O_3. The mass ratio of $BaCl_2{\cdot}2H_2O$ and Fe_2O_3 was 2:1 and the mass ratio of Fe_2O_3 and $BaFe_{12}O_{19}$ ratio was 500:1 [25]. The mixtures were calcined at 1150 °C for 8 h to synthesize plate-like $BaFe_{12}O_{19}$ powders.

Sphere-like ZnO powders were synthesized with the sol-gel method. In a typical preparation procedure, 5 g $Zn(NO_3)_2{\cdot}6H_2O$ and 3 g $NaCO_3$ were dissolved in 30 mL deionized water, respectively. The $NaCO_3$ solution was slowly added to $Zn(NO_3)_2{\cdot}6H_2O$ solution and then the viscous gels were formed. The resulting product was collected by means of centrifugation, washed repeatedly with ethanol, and dried in vacuum at 80 °C for 8 h. Finally, the product was calcined in air at 500 °C for 2 h.

Composite thick films of (1-x)ZnO/x$BaFe_{12}O_{19}$ (x = 5 wt%, 15 wt%, 25 wt%, 35 wt%) were prepared with the tape-casting method. To prepare the homogeneous slurry, the ZnO powders and $BaFe_{12}O_{19}$ powders were mixed according to different mass ratios, together with the solvent (alcohol, 60 wt% of the powders, and butanone, 90 wt% of the powders), dispersant (glycerol trioleate, 2 wt% of the powders), binder (PVB, 5 wt% of the powders) and plasticizer (dibutyl phthalate, 3 wt% of the powders). Then the tape casting was carried out with the doctor blade height of 20 μm and at a speed of 30 cm/min. The resulting ZnO/$BaFe_{12}O_{19}$ composite thick films were dried at 100 °C for 10 h.

(3) Characterization

Phase analysis of the samples was performed with an X-ray diffractometer (XRD, Rigaku D/MAX-2400, Japan) using CuKα radiation. The morphology of the samples was investigated with a field emission scanning electron microscopy (SEM, Hitachi S-4800, Japan). The magnetic properties were measured at room temperature on a vibrating sample magnetometer (VSM, Lakeshore-7410, Westerville, OH). The S parameters including S11, S12, S21 and S22 will be tested by a HP8720ES vector network analyzer using the coaxial-line method. Scheme 1 illustrates the schematic representation of typical electromagnetic parameters measurement setup. The testing samples were prepared by cutting a single layer and then pressing into toroidal-shaped samples (Øout:7.0 mm, Øin:3.04 mm). Afterward, The μ′, μ″, ε′, ε″ values of the samples were calculated with dedicated software.

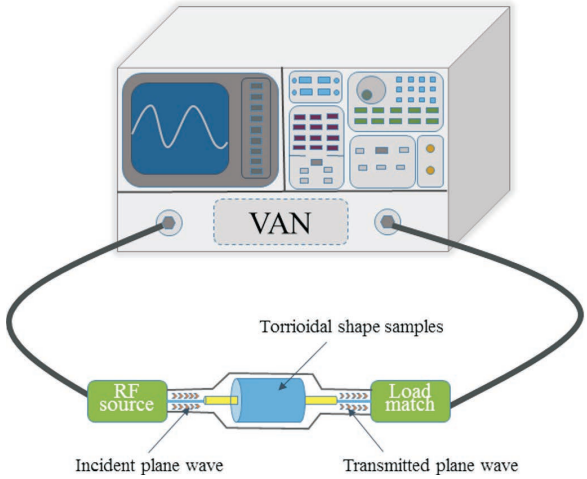

Scheme 1: Schematic representation of a typical set-up for the measurement of electromagnetic parameters.

III. Results and Discussion

The X-ray diffraction (XRD) pattern of the $BaFe_{12}O_{19}$ powders synthesized by means of MSS at 1150 °C for 4 h is provided in Fig. 1(a). This pattern shows the formation of a single phase without any traces of unwanted or parasite phases. The diffraction peaks are indexed to JCPDS card no. 43 – 0002. Most of the peaks of (00h), such as (006), (008) and (0014) are found to have higher intensities than other peaks, indicating the surface of $BaFe_{12}O_{19}$ grains is parallel to the (00h) planes. This suggests that the $BaFe_{12}O_{19}$ grains have a high degree of grain orientation, and the corresponding SEM image (inset of Fig. 1 (a)) shows that these grains have a plate-like morphology. The growth along the a(b) axis is more pronounced than that along the c-axis, owing to the diffraction peaks of (006), (008) and (0014) planes in the XRD patterns. In Fig. 1(b), the diffraction peaks at 31.8°, 34.6°, and 36.4° originate from ZnO (JCPDS card no. 36 – 1451). No diffraction peaks of other impurities are detected, which indicates a high purity and crystallinity of these ZnO samples [26]. The SEM image (inset of Fig. 1(b)) shows that the synthesized ZnO nanomaterials are globular and of uniform size.

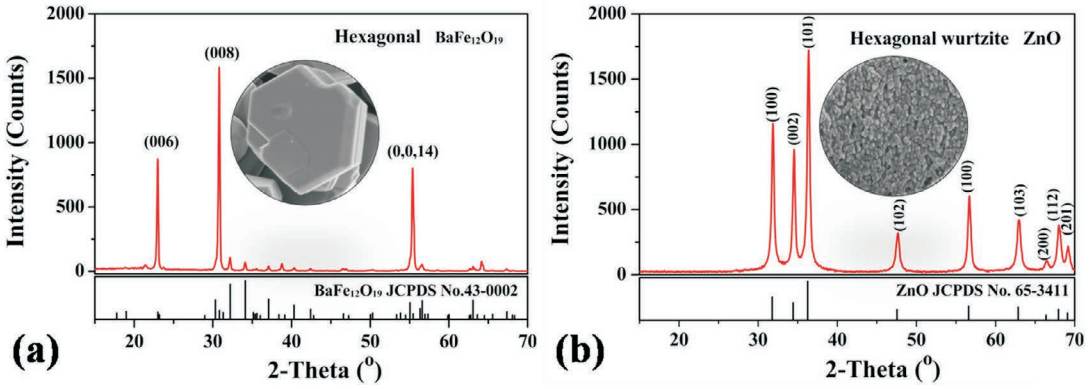

Fig. 1: XRD pattern of the $BaFe_{12}O_{19}$ and ZnO powders. The inset in (a) is a magnified local area of $BaFe_{12}O_{19}$ SEM images and the inset in (b) is an SEM image of ZnO.

The SEM micrographs of the ZnO/$BaFe_{12}O_{19}$ composite thick films with different mass fraction of $BaFe_{12}O_{19}$ are presented in Fig. 2. It can be seen that the diameters of ZnO grains in the four thick films coincide well with each other, and are about 50 – 100 nm, and the thickness and the diameter of $BaFe_{12}O_{19}$ grains are about 50 – 70 nm and 10 – 20 μm, respectively. Noticeably, $BaFe_{12}O_{19}$ grains exhibit the high degree of orientation in the films. In order to illustrate the internal structure of ZnO/$BaFe_{12}O_{19}$ composite thick films, the microstructure and structures of the representative 65 %ZnO/35 %$BaFe_{12}O_{19}$ composite thick film were investigated with a high-resolution scanning electron microscope (HRSEM), as shown in Fig. 3. From Fig. 3(a) and Fig. 3(b), it can be found that in the 65 %ZnO/35 %$BaFe_{12}O_{19}$ composite thick film, $BaFe_{12}O_{19}$ grains are evenly distributed between ZnO grains. From the energy-dispersive spectrometer (EDS) mapping image, it can be easily seen that the O, Zn, Fe and Ba are uniformly distributed, implying that the plate-like $BaFe_{12}O_{19}$ and ZnO spheres are well dispersed in the composites.

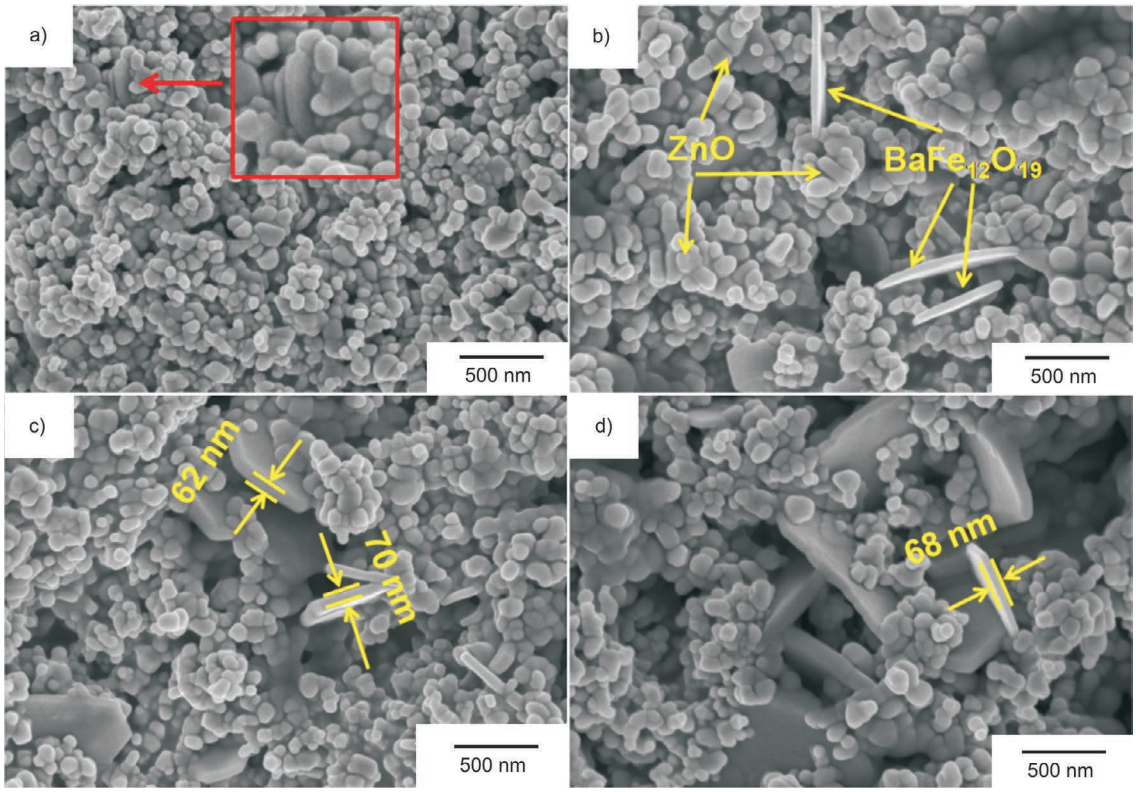

Fig. 2: SEM micrographs of the (1-x)ZnO/x$BaFe_{12}O_{19}$ composite thick films after tape casting: (a) x = 5 wt%, (b) x = 15 wt%, (c) x = 25 wt%, (d) x = 35 wt%.

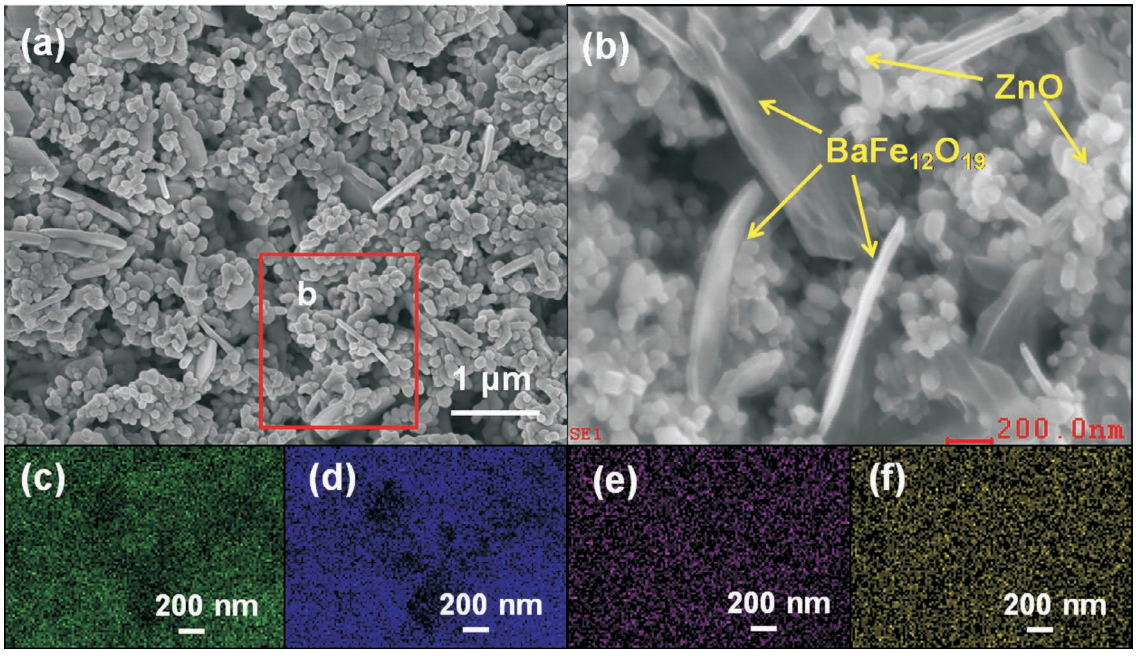

Fig. 3: SEM images of the 65 %ZnO/35 %$BaFe_{12}O_{19}$ composite thick film at different magnifications (a, b), elemental maps of O (c), Zn (d), Fe (e) and Ba (g) in ZnO/$BaFe_{12}O_{19}$ composite thick films, respectively.

To verify the magnetic properties of the samples, the hysteresis loop of each sample was measured using VSM, as shown in Fig. 4. It is shown that all the films exhibit a soft magnetic behavior. The saturation magnetization (M_s) of (1-x)ZnO/x$BaFe_{12}O_{19}$ composite thick films with the values of 6.4, 10.1, 15.5 and 20.7 emu/g have been obtained corresponding to the $BaFe_{12}O_{19}$ fractions of x = 5, 15, 25 and 35 wt%, respectively. According to Rikukawa [27], for either domain wall movement or spin rotation, the initial permeability is proportional to M_S^2. As explained above, with increasing $BaFe_{12}O_{19}$ fraction, M_s increases.

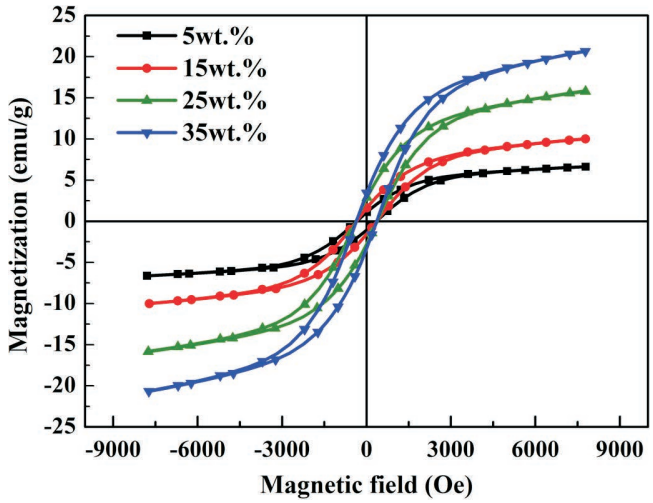

Fig. 4: Magnetization curves of $BaFe_{12}O_{19}$/ZnO composite thick films with mass fraction of $BaFe_{12}O_{19}$.

The electromagnetic parameters (relative complex permittivity, $\varepsilon_r = \varepsilon'\text{-}j\varepsilon''$, and relative complex permeability, $\mu_r = \mu'\text{-}j\mu''$) were measured to investigate the microwave absorption properties of the (1-x)ZnO/x$BaFe_{12}O_{19}$ composite thick films, as shown in Fig. 5. The real permittivity (ε') and real permeability (μ') symbolize the storage ability of electric and magnetic energy, while the imaginary permittivity (ε'') and imaginary permeability (μ'') are related to the dissipation of electric and magnetic energy [28, 29].

As shown in Fig. 5(a), both ε' and ε'' show first an increase but then decrease with the increase of the $BaFe_{12}O_{19}$ fraction in the range of 2 – 18 GHz. The ε' and ε'' of 75 wt%ZnO/25 wt%$BaFe_{12}O_{19}$ composite thick film are the highest, in the range of 15.3 – 17.2 GHz and 12.6 – 14.5 GHz, respectively. However, too high permittivity is harmful to the impedance match and results in strong reflection and weak absorption [30, 31]. In addition, the fluctuation of the ε' and ε'' in the range of 2 – 18 GHz is ascribed to displacement current lag at the heterogeneous interface. The displacement current lag is caused by the polarization process at the interfaces between ZnO and $BaFe_{12}O_{19}$ and associated relaxation process [32, 33]. The μ' and μ'' are plotted in Fig. 5(b) in the range of 2 – 18 GHz. As shown in Fig. 5(b), μ' decreases from 2.5 to 0.8 and exhibits broad multi-resonance peaks at 2 – 18 GHz, implying that natural resonance occurs in the ZnO/$BaFe_{12}O_{19}$ composite thick films. In addition, it can be speculated that the multi-resonance peaks, are the consequence of the multi-layer interface effect, the surface effect, and spin-wave excitations, defined as "exchange mode" resonance [34 – 36]. Fig. 5(c) illustrates the dielectric loss of the ZnO/$BaFe_{12}O_{19}$ composite thick films in the range of 2 – 18 GHz. It is observed that the dielectric loss first increases and then decreases with the increase of the $BaFe_{12}O_{19}$ fraction, and the dielectric loss of 75 % ZnO/25 % $BaFe_{12}O_{19}$ composite thick film is the highest. From the $\tan\delta_\mu$ curve in Fig. 5(d), it can be observed that the values of $\tan\delta_\mu$ show a decreasing tendency with increasing frequency in the range of 2 – 18 GHz, besides a slight peak found in the frequency range of 4 – 6 GHz.

Debye dipolar relaxation can be considered as an important mechanism to account for the dielectric loss of materials. The relative complex permittivity ε_r can be described as [37, 38]:

$$\varepsilon_r = \varepsilon_\infty + \frac{\varepsilon_s - \varepsilon_\infty}{1 + j2\pi f\tau} = \varepsilon' - j\varepsilon'' \quad (1)$$

where ε_s, ε_∞, f and τ are the static permittivity, relative dielectric permittivity at the high-frequency limit, frequency and polarization relaxation time, respectively. Thus, ε' and ε'' can be described by

$$\varepsilon' = \varepsilon_\infty + \frac{\varepsilon_s - \varepsilon_\infty}{1 + (2\pi f)^2\tau^2} \quad (2)$$

$$\varepsilon'' = \frac{2\pi f\tau(\varepsilon_s - \varepsilon_\infty)}{1 + (2\pi f)^2\tau^2} \quad (3)$$

According to Eq. (2) and (3), the relationship between ε' and ε'' can be deduced as

$$\left[\varepsilon' - \frac{\varepsilon_s + \varepsilon_\infty}{2}\right]^2 + (\varepsilon'')^2 = \left[\frac{\varepsilon_2 - \varepsilon_\infty}{2}\right]^2 \quad (4)$$

Thus, the plot of ε' versus ε'' would be a single semicircle, generally denoted as the Cole-Cole semicircle [39]. The Cole-Cole plot of the ZnO/$BaFe_{12}O_{19}$ composite thick films is shown in Fig. 6. Each semicircle corresponds to one Debye relaxation process. Three Cole-Cole semicircles can be found for the ZnO/$BaFe_{12}O_{19}$ composite thick films, indicating the existence of a Debye relaxation process. The three relaxation processes of the ZnO/$BaFe_{12}O_{19}$ composite thick films may arise as follows: under the alternating electromagnetic field, there is a lag of the induced charges from the interfaces of ZnO@$BaFe_{12}O_{19}$, ZnO@ZnO and $BaFe_{12}O_{19}$@$BaFe_{12}O_{19}$, which results in relaxation under the external applied field and transfers the electromagnetic energy to the thermal energy [40]. Therefore, the microwave energy is attenuated. The Cole-Cole semicircles are distorted, indicating that except for the Debye relaxation, other mechanisms, such as Maxwell-Wagner relaxation and electron polarization, could also exist in the network ZnO/$BaFe_{12}O_{19}$ composite thick films. In the network structured composites, the additional interfaces can induce interfacial polarizations [41, 42]. In addition, the numerous ZnO and $BaFe_{12}O_{19}$ particles are responsible for interfacial polarization, which further contributes to the dielectric loss. Interfacial polarization occurs in the heterogeneous media due to accumulation of charges at the interfaces.

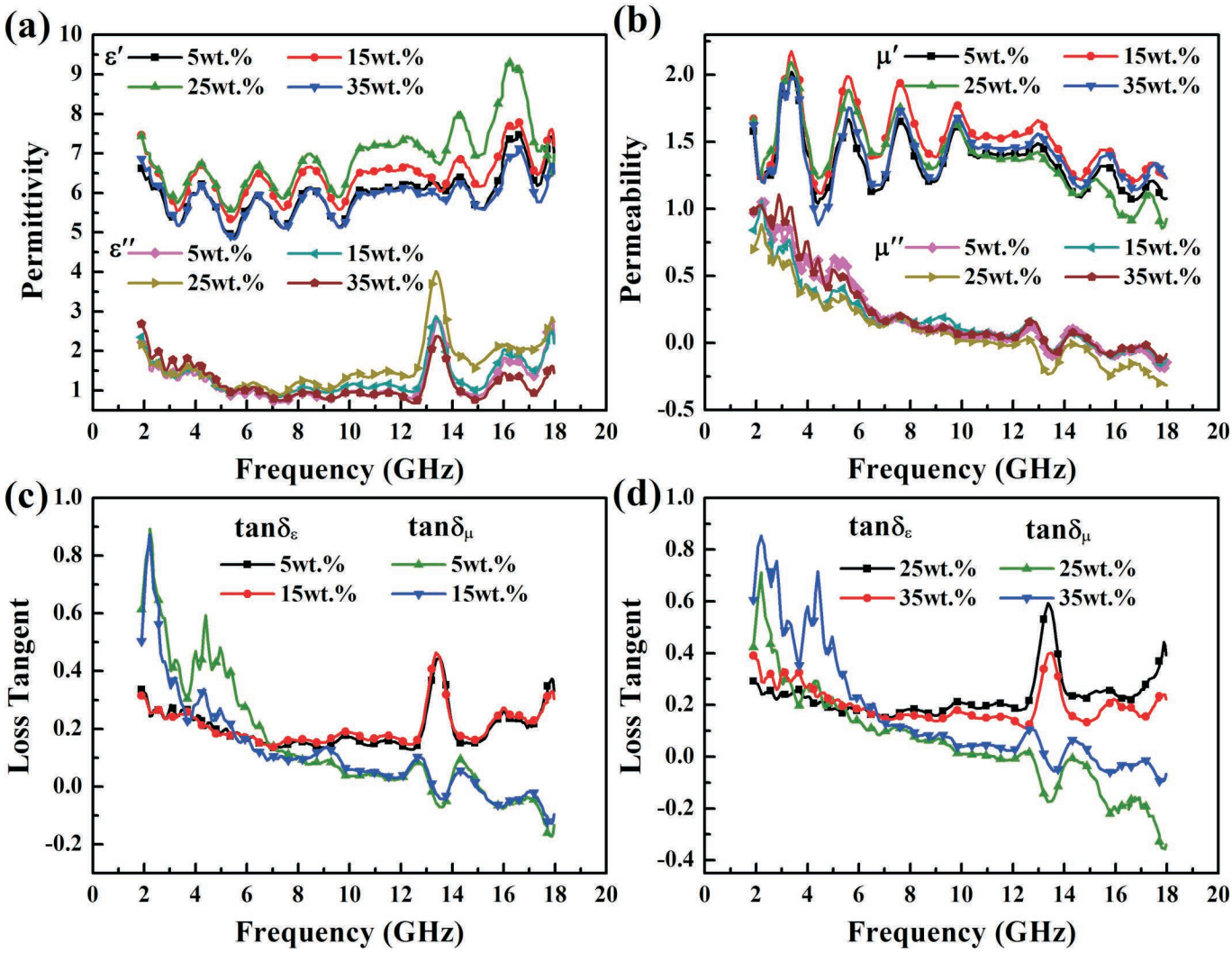

Fig. 5: Frequency dependence of permittivity (a) and permeability (b), the dielectric loss and magnetic loss (c) and (d) for ZnO/$BaFe_{12}O_{19}$ composite thick films with different mass fractions.

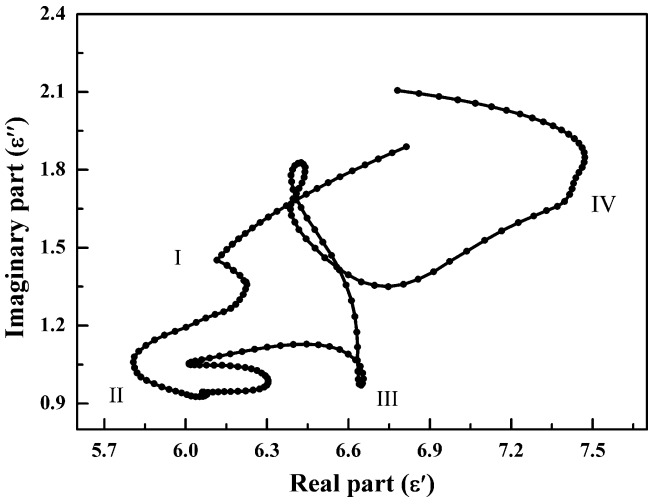

Fig. 6: The relation between the real part (ε′) and imaginary part (ε″) of complex permittivity (Cole-Cole plot) of ZnO/$BaFe_{12}O_{19}$ composite thick films.

It is well known that the magnetic loss is related to domain wall resonance [43], the eddy current effect and the natural resonance of the composite thick films [44, 45]. The contribution of domain wall resonance is negligible since it occurs usually in the low frequency range of 1 – 100 MHz, which is far lower than the measurement frequencies. The eddy current loss is related to the diameter of the particles (d) and electric conductivity (σ), which can be expressed by the following equation [46, 47]:

$$\mu'' = 2\pi\mu_0(\mu')^2\sigma d^2 f/3 \quad (5)$$

where μ_0 is the permeability of vacuum. As a deformation formula:

$$\mu''(\mu^{prime})^2 f^{-1} = 2\pi\mu_0\sigma d^2/3 = C_0 \quad (6)$$

If the magnetic loss results from eddy current loss, the value of C_0 is a constant when the frequency is varied [48].

Fig. 7 shows the eddy-current loss curves of the ZnO/$BaFe_{12}O_{19}$ composite thick films with different mass fractions of $BaFe_{12}O_{19}$, the C_0 values changes drastically as a function of frequency in the range of 2.0 – 7.0 GHz. However, it can be seen that the composite thick films have a constant $\mu''(\mu')^{-2}(f)^{-1}$ value from 7.0 to 18.0 GHz, indicating that the eddy-current loss range of the samples is wider in relatively high frequency regions. Besides, the magnetic loss in the ZnO/$BaFe_{12}O_{19}$ composite thick films is mainly caused by the natural resonance in the frequency range of 2.0 – 7.0 GHz. For the ZnO/$BaFe_{12}O_{19}$ composite thick films, the natural resonance can be attributed to

the small size effect of ZnO. According to the natural-resonance equation [49],

$$2\pi f_r = rH_\partial \tag{7}$$

$$H_\partial = \frac{4|K_1|}{3\mu_0 M_s} \tag{8}$$

where r is the gyromagnetic ratio, H_a is the anisotropy energy, and $|K_1|$ is the anisotropy coefficient. Generally, the undoped barium hexaferrite has a natural resonance frequency at about 48 GHz due to its strong uniaxial anisotropy along the c-axis [50]. According to Eq. (8), the anisotropy energy increases with the decrease of saturation magnetization. The M_s value of the ZnO/$BaFe_{12}O_{19}$ composite thick films increases with the increase of the $BaFe_{12}O_{19}$ mass fraction (Fig. 4). Hence, the H_∂ of the 65 %ZnO/35 %$BaFe_{12}O_{19}$ composite thick film is higher. The higher H_∂ is helpful to the improvement of microwave absorption properties [51].

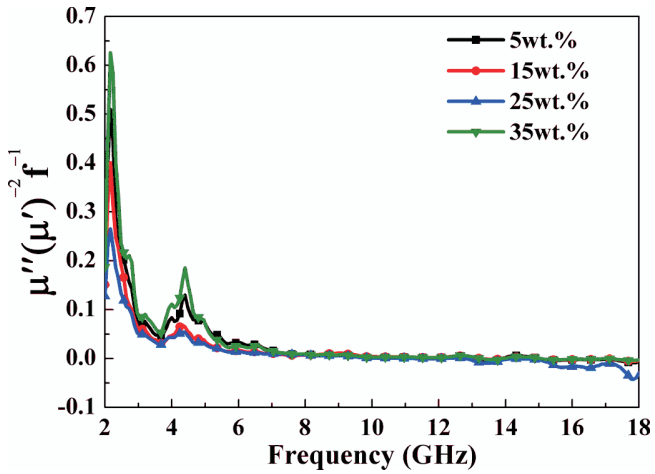

Fig. 7: Frequency dependency of the eddy-current loss curves of ZnO/$BaFe_{12}O_{19}$ composite thick films with different mass fraction of $BaFe_{12}O_{19}$.

In order to avoid the reflection of electromagnetic wave on the surface, the characteristic impedance should be as close as possible to the free space. Z_{im} can be calculated according to the complex permittivity and complex permeability, and the formula is as follows [52].

$$Z_{im} = \sqrt{\frac{\mu_0}{\varepsilon_0}}\sqrt{\frac{\mu_r}{\varepsilon_r}} \tag{9}$$

Fig. 8 shows that the Z_{im} value of the ZnO/$BaFe_{12}O_{19}$ composite thick films is 0.30 ~ 0.65 in the whole measurement frequency range, less than Z (Z = 1), which shows that the electromagnetic waves on the sample surface have a larger reflection. According to the impedance matching theory, more electromagnetic waves reflected from the surface of the sample are greatly reduced, and more electromagnetic waves can enter the interior of the material [53, 54]. In an alternating electromagnetic field, the macroscopic current would be induced to overcome the variation of the electromagnetic waves. Therefore the electromagnetic waves will be dissipated in the form of Joule heat [55].

Reflection loss (RL) represents the microwave absorption property and can be calculated from the relative permeability and permittivity at a given frequency (f) and thickness (d) using the following equations [56–58]:

$$Z_{in} = \sqrt{\frac{u_r}{\varepsilon_r}}\tanh\left(j\frac{2\pi fd}{c}\sqrt{u_r\varepsilon_r}\right) \tag{10}$$

$$RL(dB) = 20\lg\left|\frac{Z_{in}-1}{Z_{in}+1}\right| \tag{11}$$

where f is the microwave frequency, d is the thickness of the absorber, c is the velocity of light and Z_{in} is the input impedance of the absorber. The impedance matching condition is determined by the combinations of six parameters (namely, ε′, ε″, μ′, μ″, f and d). The reflection loss curve versus frequency can be calculated from ε_r and μ_r at an as-designed layer thickness.

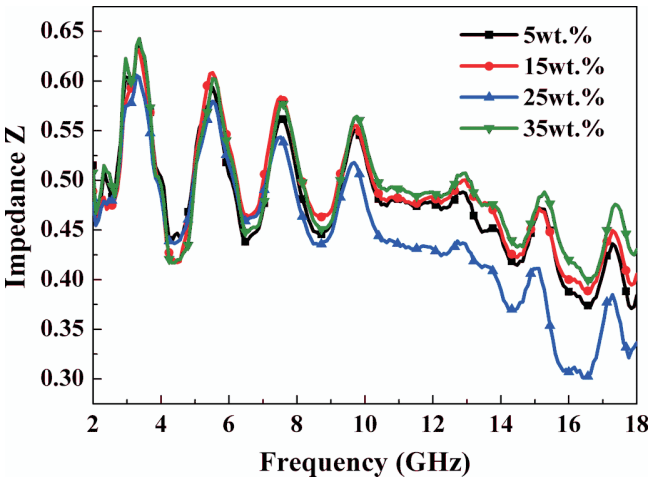

Fig. 8: The impedance of the composites versus frequency of ZnO/$BaFe_{12}O_{19}$ composite thick films with different mass fraction of $BaFe_{12}O_{19}$.

Fig. 9 shows the calculated three-dimensional presentations of theoretical RL of the ZnO/$BaFe_{12}O_{19}$ composite thick films with different thicknesses in the range of 2 – 18 GHz. The microwave absorption properties of the ZnO/$BaFe_{12}O_{19}$ composite thick films and some recently reported ZnO-based composites are shown in Table 1. As shown in Fig. 9(a), the minimum RL reaches -32.4 dB at 12.6 GHz for the 95 wt%ZnO/5 wt%$BaFe_{12}O_{19}$ composite thick film with a thickness of 6 mm, and the bandwidth of RL less than -10 dB can reach up to 5.9 GHz. For 85 wt%ZnO/15 wt%$BaFe_{12}O_{19}$ composite thick film (Fig. 9(b)), the minimum RL reaches -48.6 dB at 17.2 GHz with a thickness of 4.5 mm, whereas for 75 wt%ZnO/25 wt%$BaFe_{12}O_{19}$ composite thick film (Fig. 9(c)), the minimum RL reaches -36.0 dB at 15.3 GHz with a thickness of 5 mm. For 65 wt%ZnO/35 wt%$BaFe_{12}O_{19}$ composite thick film (Fig. 9(d)), the minimum RL reaches -36.6 dB at 12.6 GHz with a thickness of 6 mm. From the above data, it can be concluded that the ZnO/$BaFe_{12}O_{19}$ composite thick films have microwave absorption with multiple frequency bands at a certain thickness. The peak at high frequency is related to the natural resonance, and the absorption peak at low frequencies is attributed to the domain wall motion [43]. And we can infer that the microwave absorption properties of the ZnO/$BaFe_{12}O_{19}$ composite thick films can be adjusted based on the thickness and the $BaFe_{12}O_{19}$ mass fraction.

Table 1: The microwave absorption properties of ZnO/$BaFe_{12}O_{19}$ composite thick films and some recently reported composites.

Samples	Minimum RL value (dB)	Optimum thickness (mm)	Optimum frequency (GHz)	Frequency range (RL<-10dB)	Ref.
Tubular ZnO/$CoFe_2O_4$ nanocomposites	-28.2 dB	1.5 mm	8.6 GHz	9 GHz	13
$BaFe_{12}O_{19}$/ZnO composite	-37.5 dB	6.8 mm	4 GHz	4.3 GHz	2
ZnO-Based materials modified with $ZnAl_2O_4$	-25 dB	2.8mm	10.5 GHz	4.5 GHz	14
Cage-like ZnO/SiO_2 nanocomposites	-10.6dB	3.0 mm	12.8 GHz	-	18
95 wt%ZnO/5 wt%$BaFe_{12}O_{19}$	-32.4 dB	6.0 mm	12.6 GHz	5.9 GHz	this work
85 wt%ZnO/15 wt%$BaFe_{12}O_{19}$	-48.6 dB	4.5 mm	17.2 GHz	2.3 GHz	this work
75 wt%ZnO/25 wt%$BaFe_{12}O_{19}$	-36.0 dB	5.0 mm	15.3 GHz	3.8 GHz	this work
65 wt%ZnO/35 wt%$BaFe_{12}O_{19}$	-36.6 dB	6.0 mm	12.6 GHz	2.2 GHz	this work

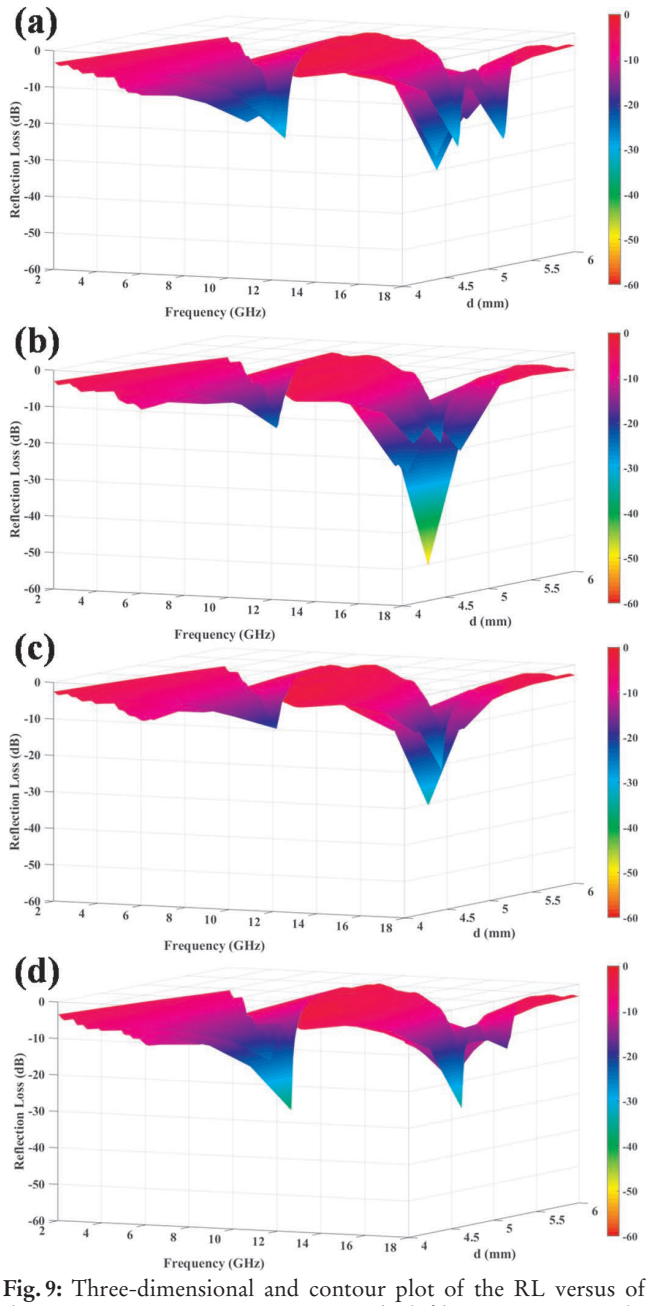

Fig. 9: Three-dimensional and contour plot of the RL versus of the (1-x)ZnO/x$BaFe_{12}O_{19}$ composite thick films (a)x = 5 wt%, (b) 15 wt%, (c) 25 wt%, (d) 35 wt%.

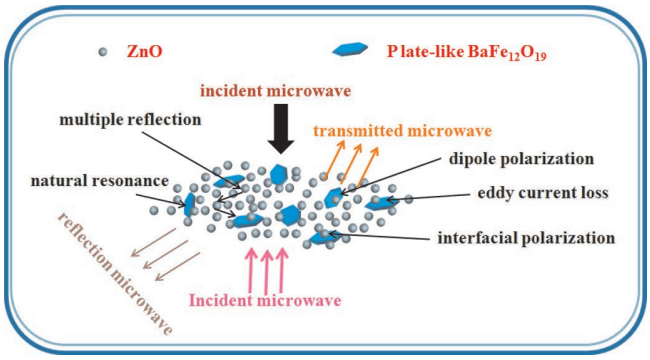

Fig. 10: Schematic illustration of possible EM absorption mechanisms in the ZnO/$BaFe_{12}O_{19}$ composite thick films.

The microwave absorption performances of the ZnO/$BaFe_{12}O_{19}$ composite thick films are mainly attributed to two key factors: electromagnetic wave attenuation and impedance matching. To give a visual demonstration of the microwave absorption mechanism, a schematic diagram is presented in Fig. 10. The three-dimensional network will be formed when the plate-like $BaFe_{12}O_{19}$ grains are distributed among the sphere-like ZnO grains. As electromagnetic waves impenetrate the thick film, the energy is induced into dissipative current by the networks, which can be explained by the following facts. Firstly, the multi-interfaces and triple junctions (ZnO@$BaFe_{12}O_{19}$, ZnO@ZnO, $BaFe_{12}O_{19}$@$BaFe_{12}O_{19}$) are advantageous for electromagnetic attenuation owing to the existing interfacial polarizations [59, 60]. The electromagnetic waves radiating on absorbents are partially absorbed, while the surplus electromagnetic waves will present diffuse reflections owing to the multiple interfaces. During the process of diffuse reflections, the electromagnetic waves enter another process, in which the energy is induced into dissipative current. Secondly, the $BaFe_{12}O_{19}$ grains and the void space existing between ZnO and $BaFe_{12}O_{19}$ grains result in relatively large specific surface areas, providing more active sites for reflection and scattering of electromagnetic waves [61]. Finally, the void space between ZnO and $BaFe_{12}O_{19}$ grains can effectively interrupt the spread of electromagnetic waves and generate dissipation owing to the existing impendence difference and enhance the

microwave absorption properties [62]. The results could provide guidance for exploring and designing advanced microwave absorption materials based on adjustment of the $BaFe_{12}O_{19}$ mass fraction and the thickness of the composite thick films.

IV. Conclusions

In conclusion, $ZnO/BaFe_{12}O_{19}$ composite thick films have been successfully synthesized with the tape-casting process with the presence of synthesized plate-like $BaFe_{12}O_{19}$ grains and ZnO sphere-like grains, in which interweaves with ZnO spheres and a three-dimensional network can be formed. The phase composition, morphology and magnetic properties of the $ZnO/BaFe_{12}O_{19}$ composite thick films are also characterized and discussed. The electromagnetic data demonstrate that the microwave absorption property of the thick films can be adjusted easily by varying the mass ratio of $BaFe_{12}O_{19}$. When the mass ratio of $BaFe_{12}O_{19}$ is 15, the composite thick film exhibits a minimum RL of -48.6 dB at 17.2 GHz with a thickness of 4.5 mm. Such composite thick films could be developed for a wide spectrum of applications in the area of microwave absorption.

Acknowledgements

This work is supported by the National Natural Science Foundation of China (Grant No. 51772177), the Chinese Postdoctoral Science Foundation (Grant No. 2016M590916), the Scientific Research Foundation for Returned Overseas Chinese Scholars, State Education Ministry, the Science and Technology Foundation of Weiyang District of Xi'an City (Grant No. 201605), the Industrialization Foundation of Education Department of Shaanxi Provincial Government (Grant No. 16JF002)

References

1 Hwang, Y.: Microwave absorbing properties of NiZn-ferrite synthesized from waste iron oxide catalyst, *Mater. Lett.*, **60**, 3277 – 3280, (2006).

2 Chen, W., Zheng, J., Li, Y.: Synthesis and electromagnetic characteristics of $BaFe_{12}O_{19}$/ZnO composite material, *J. Alloy. Compd.*, **513**, 420 – 424, (2012).

3 Al-Ghamdi, A.A., Al-Ghamdi, A.A., Al-Turki, Y., Yakuphanoglu, F., El-Tantawy, F.: Electromagnetic shielding properties of graphene/acrylonitrile butadiene rubber nanocomposites for portable and flexible electronic devices, *Compos. Part B- Eng.*, **88**, 212 – 219, (2016).

4 Al-Ghamdi, A.A., Al-Hartomy, O.A., Al-Solamy, F.R., Dishovsky, N., Malinova, P., Atanasova, G., Atanasovde, N.: Conductive carbon black/magnetite hybrid fillers in microwave absorbing composites based on natural rubber, *Compos. Part B-Eng.*, **96**, 231 – 241, (2016).

5 Yang, C.C., Gung, Y.J., Hung, W.C., Ting, T.H., Wu, K.H.: Infrared and microwave absorbing properties of $BaTiO_3$/polyaniline and $BaFe_{12}O_{19}$/polyaniline composites, *Compos. Sci. Technol.*, **70**, 466 – 471, (2010).

6 Kong, L., Yin, X.W., Han, M.K., Yuan, X.Y., Hou, Z.X., Ye, F., Zhang, L.T., Cheng, L.F., Xu, Z.W., Huang, J.F.: Macroscopic bioinspired graphene sponge modified with *in-situ* grown carbon nanowires and its electromagnetic properties, *Carbon*, **111**, 94 – 102, (2017).

7 Gashti, M.P., Almasian, A.: Synthesizing tertiary silver/silica/kaolinite nanocomposite using photo-reduction method: characterization of morphology and electromagnetic properties, *Compos. Part B-Eng.*, **43**, 3374 – 3383, (2012).

8 Zhuo, R.F., Qiao, L., Feng, H.T., Chen, J.T., Yan, D., Wu, Z.G., Yan, P.X.: Microwave absorption properties and the isotropic antenna mechanism of ZnO nanotrees, *J. Appl. Phys.*, **104**, 94101 – 94105, (2008).

9 Chen, Y.J., Cao, M.S., Wang, T.H., Wan, Q.: Microwave absorption properties of the ZnO nanowire-polyester composites, *Appl. Phys. Lett.*, **84**, 367 – 369, (2004).

10 Choi, W.H., Kim, C.G.: Broadband microwave-absorbing honeycomb structure with novel design concept, *Compos. Part B-Eng.*, **83**, 14 – 20, (2015).

11 Hu, Q., Tong, G., Wu, W., Liu, F.T., Qian, H.S., Hong, D.Y.: Selective preparation and enhanced microwave electromagnetic characteristics of polymorphous ZnO architectures made from a facile one-step ethanediamine-assisted hydrothermal approach, *CrystEngComm*, **15**, 1314 – 1323, (2013).

12 Singhal, R.K., Samariya, A., Xing, Y.T., Kumar, S., Dolia, S.N., Deshpande, U.P., Shripathi, T., Saitovitchb, E.B.: Electronic and magnetic properties of Co-doped ZnO diluted magnetic semiconductor, *J. Alloy. Compd.*, **496**, 24 – 30, (2010).

13 Zhuo, R.F., Qiao, L., Feng, H.T., Chen, J.T., Yan, D., Wu, Z.G., Yan, P.X.: Microwave absorption properties and the isotropic antenna mechanism of ZnO nanotrees, *J. Appl. Phys.*, **104**, 119.– 123, (2008).

14 Jiang, J., Ai, L.H.: $SrFe_{12}O_{19}$/ZnO hybrid structures: synthesis, characterization and properties, *J. Alloy. Compd.*, **502**, 88 – 90, (2010).

15 Cao, J., Fu, W., Yang, H., Yu, Q., Zhang, Y., Liu, S., Sun, P., Zhou, X., Leng, Y., Wang, S., Liu, B., Zou, G.: Large-scale synthesis and microwave absorption enhancement of actinomorphic tubular $ZnO/CoFe_2O_4$ nanocomposites, *J. Phys. Chem., B*, **113**, 4642 – 4647, (2009).

16 Kong, L., Yin, X., Ye, F., Li, Q., Zhang, L.T., Cheng, L.F.: Electromagnetic wave absorption properties of ZnO-based materials modified with $ZnAl_2O_4$ nanograins, *J. Phys. Chem. C*, **117**, 2135 – 2146, (2013).

17 Xu, P., Han, A.X.J., Wang, M.: Synthesis and magnetic properties of $BaFe_{12}O_{19}$ hexaferrite nanoparticles by a reverse microemulsion technique, *J. Phys. Chem. C*, **111**, 5866 – 5870, (2007).

18 Yu, H.F., Liu, P.C.: Effects of pH and calcination temperatures on the formation of citrate-derived hexagonal barium ferrite particles, *J. Alloy. Compd.*, **416**, 222 – 227, (2006).

19 Paul, K.B.: Magnetic and structural properties of ba M-type ferrite-composite powders, *Physica. B*, **388**, 337 – 343, (2007).

20 Cao, M.S., Shi, X.L., Fang, X.Y., Jin, H.B.: Microwave absorption properties and mechanism of cage-like ZnO/SiO_2, nanocomposites, *Appl. Phys. Lett.*, **91**, 203110 – 203113, (2007).

21 Watanabe, H., Kimura, T., Yamaguchi, T.: Particle orientation during tape casting in the fabrication of grain-oriented bismuth titanate, *J. Am. Ceram. Soc.*, **72**, 289 – 293, (1989).

22 Ni, D.W., Schmidt, C.G., Teocoli, F., Kaiser, A., Andersen, K.B., Ramousse, S., Esposito, V.: Densification and grain growth during sintering of porous $Ce_{0.9}Gd_{0.1}O_{1.95}$, tape cast layers: A comprehensive study on heuristic methods, *J. Eur. Ceram. Soc.*, **33**, 2529 – 2537, (2013).

23 Wang, L., Tang, G., Xu, Z.K.: Preparation and electrical properties of multilayer ZnO varistors with water-based tape casting, *Ceram. Int.*, **35**, 487 – 492, (2009).

24 Albano, M.P., Garrido, L.B.: Aqueous tape casting of yttria stabilized zirconia, *Mat. Sci. Eng. A*, **420**, 171 – 178, (2006).

25 Hovis, D.B., Faber, K.T.: Textured microstructures in barium hexaferrite by magnetic field assisted gelcasting and templated grain growth, *Scr. Mater.*, **44**, 2525 – 2529, (2001).

26 Lanje, A.S., Sharma, S.J., Ningthoujam, R.S., Ahn, J.S., Pode, R.B.: Low temperature dielectric studies of zinc oxide (ZnO)

nanoparticles prepared by precipitation method, *Adv. Powder Technol.*, **24**, 331 – 335, (2013).

27 Rikukawa, H.: Relationship between microstructures and magnetic properties of ferrites containing closed pores, IEEE Mag., **18**, 1535 – 1537, (1982).

28 Luo, H., Shen, J., Zhang, C.: Synthesis and microwave absorbing mechanism of two-layer microwave absorbers containing $Li_{0.35}Zn_{0.3}Fe_{2.35}O_4$, micro-belts and nickel-coated carbon fibers, *Compos. Part B-Eng.*, **50**, 62 – 66, (2013).

29 Bora, P.J., Azeemb, I., Vinoy, K.J., Ramamurthy, P.C., Madrasa, G.: Morphology controllable microwave absorption property of polyvinylbutyral (PVB)-MnO_2 nanocomposites, *Compos. Part B-Eng.*, **132**, 188 – 196, (2018).

30 Shan, L., Chen, X.N., Tian, X., Chen, J.J., Zhou, Z.W., Jiang, M., Xua, X.L., Hui, D.: Fabrication of polypyrrole/nano-exfoliated graphite composites by *in situ* intercalation polymerization and their microwave absorption properties, *Compos. Part B-Eng.*, **73**, 181 – 187, (2015).

31 Zhong, B., Wang, C.J., Wen, G.W., Yu, Y.L., Xia, L.: Facile fabrication of boron and nitrogen co-doped carbon@Fe_2O_3/Fe_3C/Fe nanoparticle decorated carbon nanotubes three-dimensional structure with excellent microwave absorption properties, *Compos. Part B-Eng.*, **132**, 141 – 150, (2018).

32 Tang, X., Hu, K.: Preparation and electromagnetic wave absorption properties of Fe-doped zinc oxide coated barium ferrite composites, *Mat. Sci. B-Eng.*, **139**, 119 – 123, (2007).

33 Liu, X.G., Geng, D.Y., Meng, H., Shang, P.J., Zhang, Z.D.: Microwave-absorption properties of ZnO-coated iron nanocapsules, *Appl. Phys. Lett.*, **92**, 64 – 67, (2008).

34 Zhang, X.F., Dong, X.L., Huang, H., Lu, B., Zhu, X.G., Lei, J.P., Ma, S., Liu, W., Zhang, Z.D.: Synthesis, structure and magnetic properties of SiO_2-coated fe nanocapsules, *Mat. Sci. Eng. A*, **454**, 211 – 215, (2007).

35 Aharoni, A.: Effect of surface anisotropy on the exchange resonance modes, *J. Appl. Phys.*, **81**, 830 – 833, (1997).

36 Mercier, D., Lévy, J.C.S., Viau, G., Fiévet-Vincent, F., Fiévet, F., Toneguzzo, P., Acher, O.: Magnetic resonance in spherical co-ni and fe-co-ni particles, *Phys. Rev. B*, **62**, 532 – 544, (2000).

37 He, S., Wang, G.S., Lu, C., Liu, J., Wen, B., Liu, H., Guo, L., Cao, M.S.: Enhanced wave absorption of nanocomposites based on the synthesized complex symmetrical CuS nanostructure and poly (vinylidene fluoride), *J. Mater. Chem. A*, **1**, 4685 – 4692, (2013).

38 Chen, D., Quan, H., Wang, G., Guo, L.: Hollow-MnS spheres and their hybrids with reduced graphene oxide: synthesis, microwave absorption, and lithium storage properties, *Chempluschem*,**78**, 843 – 851, (2013).

39 Zhao, B., Shao, G., Fan, B., Zhao, W., Xie, Y., Zhang, R.: Facile preparation and enhanced microwave absorption properties of core-shell composite spheres composited of ni cores and TiO_2 shells, *Phys. Chem. Chem. Phys.*, **17**, 8802 – 8810, (2015).

40 Zhang, X.J., Wang, G.S., Cao, W.Q., Wei, Y.Z., Liang, J.F., Guo, L., Cao, M.S.: Enhanced microwave absorption property of reduced graphene oxide (RGO)-$MnFe_2O_4$ nanocomposites and polyvinylidene fluoride, *ACS Appl. Mater. Inte.*, **6**, 7471 – 7478, (2014).

41 Shuai, H., Chang, L., Wang, G.S., Wang, J.W., Guo, H.Y., Guo, L.: Synthesis and growth mechanism of white-fungus-like nickel sulfide microspheres, and their application in polymer composites with enhanced microwave-absorption properties, *Chempluschem*, **79**, 569 – 576, (2014).

42 Weng, X., Li, B., Zhang, Y., Lv, X., Gu, G.: Synthesis of flake shaped carbonyl iron/reduced graphene oxide/polyvinyl pyrrolidone ternary nanocomposites and their microwave absorbing properties, *J. Alloy. Compd.*, **695**, 508 – 519, (2017).

43 Ghasemi, A.: Remarkable influence of carbon nanotubes on microwave absorption characteristics of strontium ferrite/CNT nanocomposites, *J. Magn. Magn. Mater.*, **323**, 3133 – 3037, (2011).

44 Alam, R.S., Moradi, M., Rostami, M., Nikmanesha, H., Moayedia, R., Bai, Y.: Structural, magnetic and microwave absorption properties of doped Ba-hexaferrite nanoparticles synthesized by co-precipitation method, *J. Magn. Magn. Mater.*, **381**, 1 – 9, (2015).

45 Gordani, G.R., Ghasemi, A., Saidi, A.: Optimization of carbon nanotubes volume percentage for enhancement of high frequency magnetic properties of $SrFe_8MgCoTi_2O_{19}$/MWCNTs, *J. Magn. Magn. Mater.*, **363**, 49 – 54, (2014).

46 Zhu, W., Wang, L., Zhao, R., Ren, J., Lu, G., Wang, Y.: Electromagnetic and microwave-absorbing properties of magnetic nickel ferrite nanocrystals, *Nanoscale*, **3**, 2862 – 2864, (2011).

47 Bora, P.J., Mallik, N., Ramamurthy, P.C., Kishore, Madras, G.: Poly(vinyl butyral) -polyaniline-magnetically functionalized fly ash cenosphere composite film for electromagnetic interference shielding, *Compos. Part B-Eng.*, **106**, 224 – 233, (2016).

48 Zhang, X.F., Dong, X.L., Huang, H., Liu, Y.Y.: Microwave absorption properties of the carbon-coated nickel nanocapsules, *Appl. Phys. Lett.*, **89**, 053115 – 053118, (2006).

49 Chen, Y.J., Gao, P., Wang, R.X., Ouyang, Q.Y., Qi, L.H., Ma, Y., Gao, P., Zhu, C.L., Cao, M.S., Jin, H.B.: Porous Fe_3O_4/SnO_2 core/shell nanorods: synthesis and electromagnetic properties, *J. Phys. Chem. C*, **113**, 10061 – 10064, (2009).

50 Asghari, M., Ghasemi, A., Paimozd, E., Morisako, A.: Evaluation of microwave and magnetic properties of substitutted $SrFe_{12}O_{19}$, and substituted $SrFe_{12}O_{19}$/multi-walled carbon nanotubes nanocomposites, *Mater. Chem. Phys.*, **143**, 161 – 166, (2013).

51 Chen, T., Qiu, J., Zhu, K., Che, Y.C., Zhang, Y., Zhang, J.M., Li, H., Wang, F., Wang, Z.Z.: Enhanced electromagnetic wave absorption properties of polyaniline-coated Fe_3O_4/reduced graphene oxide nanocomposites, *J. Mater. Sci.*, **25**, 3664 – 3673, (2014).

52 Zheng, G., Yin, X., Liu, S., Liu, X.M., Deng, J.L., Li, Q.: Improved electromagnetic absorbing properties of Si_3N_4-SiC/SiO_2 composite ceramics with multi-shell microstructure, *J. Eur. Ceram. Soc.*, **33**, 2173 – 2180, (2013).

53 Tang, H., Jian, X., Wu, B., Liu, S.Y., Jiang, Z.C., Chen, X.G., Lv, W.Q., He, W.D., Tian, W., Wei, Y.F., Gao, Y.Q., Chen, T., Li, G.: Fe_3C/helical carbon nanotube hybrid: facile synthesis and spin-induced enhancement in microwave-absorbing properties, *Compos. Part B-Eng.*, **107**, 51 – 58, (2016).

54 Kong, L., Wang, C., Yin, X.W., Fan, X.M., Wang, W., Huang, J.F.: Electromagnetic wave absorption properties of a carbon nanotube modified by a tetrapyridinoporphyrazine interface layer, *J. Mater. Chem. C*, **5**, 7479 – 7488, (2017).

55 Mondal, S., Ganguly, S., Das, P., Khastgir, D., Das, N.C.: Low percolation threshold and electromagnetic shielding effectiveness of nano-structured carbon based ethylene methyl acrylate nanocomposites, *Compos. Part B-Eng.*, **119**, 41 – 56, (2017).

56 Bai, X., Zhai, Y., Zhang, Y.: Green approach to prepare graphene-based composites with high microwave absorption capacity, *J. Phys. Chem. C*, **115**, 11673 – 11677, (2011).

57 Melvin, G.J.H., Ni, Q.Q., Narsuki, T.: Electromagnetic wave absorption properties of barium titanate/carbon nanotube hybrid nanocomposites, *J. Alloy. Compd.*, **615**, 84 – 90, (2014).

58 Lv, H., Ji, G., Wang, M., Shang, C.M., Zhang, H.Q., Du, Y.W.: Hexagonal-cone like of $Fe_{50}Co_{50}$, with broad frequency microwave absorption: effect of ultrasonic irradiation time, *J. Alloy. Compd.*, **615**, 1037 – 1042, (2014).

59 Yang, X., Wang, X., Liu, X., Zhang, Y., Song, W., Shu, C., Jiang, L., Wang, C.: Preparation of graphene-like iron oxide nanofilm/silica composite with enhanced adsorption and efficient photocatalytic properties, *J. Mater. Chem. A*, **1**, 8332 – 8337, (2013).

[60] Bibi, M., Abbas, S.M., Ahmad, N., Muhammada, B., Iqbald, Z., liRanae, U.A., Salah, Khane, U.D.: Microwaves absorbing characteristics of metal ferrite/multiwall carbon nanotubes nanocomposites in X-band, *Compos. Part B-Eng.*, **114**, 139 – 148, (2017).

[61] Qi, X.S., Zhong, W., Deng, Y., Au, C.K.T., Du, Y.W.: Characterization and magnetic properties of helical carbon nanotubes and carbon nanobelts synthesized in acetylene decomposition over Fe-Cu nanoparticles at 450 °C, *J. Phys. Chem. C*, **113**, 1303 – 1306, (2009).

[62] Qin, Y., Che, R., Liang, C., Zhang, J., Wen, Z.: Synthesis of au and Au-CuO cubic microcages via an *in situ* sacrificial template approach, *J. Mater. Chem.*, **21**, 3960 – 3965, (2011).